Journal of Glaciology

Article

Cite this article: Ockenden H, Bingham RG, Curtis A, Goldberg D (2023). Ice-flow perturbation analysis: a method to estimate ice-sheet bed topography and conditions from surface datasets. *Journal of Glaciology* **69**(278), 1677–1686. https://doi.org/10.1017/jog.2023.50

Received: 21 November 2022
Revised: 24 May 2023
Accepted: 16 June 2023
First published online: 3 August 2023

Keywords:
Antarctic glaciology; ice-sheet modelling; subglacial processes

Corresponding author:
Helen Ockenden;
Email: h.ockenden@sms.ed.ac.uk

cambridge.org/jog

Ice-flow perturbation analysis: a method to estimate ice-sheet bed topography and conditions from surface datasets

Helen Ockenden, Robert G Bingham, Andrew Curtis and Daniel Goldberg

School of GeoSciences, University of Edinburgh, Drummond St, Edinburgh, EH8 9XP, United Kingdom

Abstract

One of the largest contributors to uncertainty in predictions of sea-level rise from ice-sheet models is a lack of knowledge about the bed topography beneath ice sheets. Bed topography maps are normally made by interpolating between linear radar surveys using methods that include kriging, mass conservation and flowline diffusion, all of which may miss influential mesoscale (2–30 km) bedforms. Previous works have explored an Ice-Flow Perturbation Analysis (IFPA) approach for estimating bed topography using the surface expression of these mesoscale bedforms. Using regions of Pine Island Glacier that have been intensively surveyed by ice-penetrating radar as test sites, and a refined IFPA methodology, we find that IFPA detects bedforms capable of influencing ice flow which are not represented in Bedmachine Antarctica and other interpolated bed products. We further explore the ability of IFPA to estimate relative bed slipperiness, finding higher slipperiness in the main trunk and tributaries. Alongside other methods which estimate ice thickness, bed topography maps from IFPA have the potential to constrain projections of future sea-level rise, especially where radar data are sparse.

1. Introduction

Detailed knowledge of bed topography beneath ice sheets is an important input for modelling future ice-sheet behaviour and its contribution to sea-level rise. Direct measurements of bed topography have been made by radar sounding, but typically do not provide the density of coverage required by ice-sheet models. Traditionally, in slower-flowing ice, interpolation methods such as kriging and plate splines have been used to fill in the gaps (Fretwell and others, 2013), but these methods often have large uncertainties in regions where radar lines are sparse. In fast-flowing ice near the grounding line, the physical principle of mass conservation has been used to fill in the gaps (Morlighem and others, 2020). In many other upstream regions of Antarctica, a more complex interpolation method, flowline diffusion, has exploited the ice-surface flow direction to constrain the bed topography (Morlighem and others, 2020). However, the topography products from interpolation methods may miss mesoscale subglacial topography which is important for ice flow but which does not intersect radar survey lines. It is well known that variability in bed topography and basal slipperiness is transferred to the surface by ice flow (e.g. De Rydt and others, 2013; Cooper and others, 2019). High-resolution observations of ice-surface elevation may therefore provide an alternative route for recovering subglacial topography, even in regions with sparse radar coverage.

The relationship between surface and bed topography was first described mathematically by Nye (1959), and developed further by Budd (1970); Whillans and Johnsen (1983); Balise and Raymond (1985) and Reeh (1987). Gudmundsson (2003) and Gudmundsson (2008) built on these early works using a linearised perturbation analysis to provide analytical functions that describe the transfer of variability between bed topography and the ice surface. These transfer functions have been applied in 2D to bed topography on flowlines at Rutford Ice Stream (De Rydt and others, 2013) and in Greenland (Ng and others, 2018; Ignéczi and others, 2018).

For three dimensions, this linear perturbation analysis approach was first applied to MacAyeal Ice Stream by Thorsteinsson and others (2003) but, due to the low availability of high-resolution surface topography and velocity measurements at the time, it was not applied more widely. We recently built upon these foundations to apply an updated version of this methodology to modern satellite datasets across Thwaites Glacier (Ockenden and others, 2022), and we call this methodology Ice-Flow Perturbation Analysis (IFPA). Here, we present a more efficient version of the code which now also accounts for variation in ice-flow direction, and implements a full-Stokes version of the analytical functions describing the transfer of variability between bed topography and the ice surface, rather than the shallow-ice-stream approximation version used previously. In Ockenden and others (2022), ice flow was assumed to be parallel to the polar stereographic grid in the negative x direction across the whole of the main trunk of Thwaites Glacier. Although this is a passable approximation for that region, it is obviously inappropriate for other regions of Antarctica, and so in this paper's more advanced iteration of the IFPA code ice-flow direction is allowed to vary independently in each subdomain. Ice flow which is not aligned to the polar stereographic grid is accounted for by interpolating the ice surface data onto a grid aligned to the mean ice velocity, running the analysis, and then interpolating back to the polar stereographic grid. We apply IFPA to invert for

subglacial topography and slipperiness at Pine Island Glacier. We selected this region for both its overall scientific significance and because within the catchment there exist several high-resolution radar surveys of bed topography (Bingham and others, 2017) which were not included in Bedmachine Antarctica (Morlighem and others, 2020) and hence provide independent sites for testing the success of our inversions. We therefore use these high-resolution radar surveys to assess the performance of IFPA relative to current interpolated products. We also produce broad-scale estimates of the variability in relative basal slipperiness across the glacier trunk, which potentially inform values of basal slipperiness to be applied when using this method in other regions of Antarctica.

2. Methodology

2.1. Ice-Flow Perturbation Analysis (IFPA)

The IFPA method is based on the observation that perturbations in the bed topography and basal slipperiness beneath flowing ice create variability in the ice-surface topography and velocity. Perturbations in bed topography and perturbations in basal slipperiness have different effects on the ice surface velocity and elevation, and so they can be resolved separately without mixing effects (Gudmundsson and Raymond, 2008). Gudmundsson (2003) and Gudmundsson (2008) considered the physics of such perturbations in an ice slab with constant viscosity and isotropic rheology, and derived a mathematical framework for understanding the relationship between the bed and the ice surface. This forms the basis for the work that we present here.

As in Ockenden and others (2022) (see Section 2 of that paper), we consider the steady-state spatial variability of the ice-surface elevation s, ice-surface velocity parallel to flow u and perpendicular to flow v, bed topography b, and basal slipperiness c, as functions of the spatial coordinates x and y. We denote the Fourier transforms of these with a circumflex $\hat{}$, such that:

$$\hat{s}(k, l) = \int_{-\infty}^{\infty}\int_{-\infty}^{\infty} s(x, y)\mathrm{e}^{-2\pi ikx}\mathrm{e}^{-2\pi ily}\mathrm{d}x\mathrm{d}y, \quad (1)$$

where k and l are wavenumbers in the direction of flow (x) and perpendicular to the flow (y), respectively. So that we can make more general statements about the behaviour of the system in terms of variables such as ice thickness, we non-dimensionalise these parameters, and denote the non-dimensionalised quantities with a capital letter (see Ockenden and others (2022), Section 2.1.3).

For ice in a planar slab aligned in the direction of ice flow, the non-dimensionalised Fourier transforms of perturbations in ice-surface elevation and velocity can be calculated from the non-dimensionalised Fourier transforms of perturbations in bed topography and basal slipperiness:

$$\Delta\hat{S}(k, l) = T_{SB}(k, l)\,\Delta\hat{B}(k, l) + T_{SC}(k, l)\,\Delta\hat{C}(k, l), \quad (2)$$

$$\Delta\hat{U}(k, l) = T_{UB}(k, l)\,\Delta\hat{B}(k, l) + T_{UC}(k, l)\,\Delta\hat{C}(k, l), \quad (3)$$

$$\Delta\hat{V}(k, l) = T_{VB}(k, l)\,\Delta\hat{B}(k, l) + T_{VC}(k, l)\,\Delta\hat{C}(k, l), \quad (4)$$

where T_{sb}, T_{sc}, T_{ub}, T_{uc}, T_{vb}, T_{vc} are wavenumber-specific, non-dimensional transfer functions that describe the amplitude ratio of perturbations in the bed properties relative to the ice surface properties, and which vary with angle of surface slope α, sliding law parameter m and mean non-dimensional bed slipperiness $\bar{C}$. Depending on whether full-Stokes flow (Gudmundsson, 2003) or the shallow-ice-stream approximation (Gudmundsson, 2008) are considered, these transfer functions take different functional forms. Both sets of equations are set out in the Supplementary Information, and the code provided can be run with either. Due to their more complex functional form, the full-Stokes transfer functions take approximately twice as long to run.

Equations (2), (3) and (4) form an over-determined system of three known variables which can be solved using a weighted least-squares inversion (see Thorsteinsson and others, 2003, Section 3 and Ockenden and others, 2022, Appendix C). The least-squares inversion runs over a defined grid where the parameters which influence the transfer functions (mean ice thickness $\bar{h}$, angle of slope α, sliding law parameter m and mean bed slipperiness $\bar{c}$) should be approximately constant. As in Ockenden and others (2022), the mean ice thickness, $\bar{h}$, is obtained from a 50 km averaged version of BedMachine Antarctica ice thickness (Morlighem and others, 2020). In order to apply the method across a large area over which these parameters are variable, we run the model on overlapping 25 km by 25 km patches, and allow these patches to have different parameters. Each grid point in the larger area is included in nine overlapping patches, and the final elevation included in the results is the weighted mean of these nine values, with a weighting factor based on the position in the overlapping patch. This weighted smoothing reduces the number of overlapping patches required to remove most edge effects, which means that the code runs more efficiently compared to the iteration method used in Ockenden and others (2022).

2.2. Assessing method performance through comparison to radar surveys

IFPA produces maps of variations in both bed topography and basal slipperiness. However, since there are no direct observations of bed slipperiness (which is a parameter representing many components of hydrology, geology and sedimentology that cannot be independently constrained), we focus on the bed topography component of these results to test the performance of IFPA. We compare our results with ice-penetrating radar surveys of the bed topography at seven sites in Pine Island Glacier surveyed in 2010 and 2013/14 (Bingham and others, 2017). These surveys acquired data with a 500 m line spacing between ice-flow-orthogonal survey tracks, and an along-track sounding interval of 4–6 m, over regions of 20 by 40 km (2010 survey) and 10 by 15 km (all six 2013/14 surveys). Further details of acquisition and processing are detailed in Bingham and others (2017). These radar soundings were not processed in time for inclusion in BedMap2 (Fretwell and others, 2013) or Bedmachine Antarctica v1 (Morlighem and others, 2020), and so provide an opportunity to assess the performance of IFPA in emulating directly measured and previously interpolated bed topography.

We used IFPA to invert surface elevation from REMA (Howat and others, 2019) and surface velocities from ITS_LIVE (Gardner and others, 2018) for bed topography and slipperiness across the main trunk of Pine Island Glacier. IFPA performance is assessed by comparison with the directly surveyed bed topography sounded by the ice-penetrating radar, and with bed topography from Bedmachine Antarctica that, for all of these sites, was derived with flowline diffusion (Morlighem and others, 2020).

2.3. Exploring the role of the tuneable slipperiness parameter $\bar{C}$

The amplitude of variations in the topography on the surface of flowing ice sheets depends not only on the bed topography, but

https://doi.org/10.1017/jog.2023.50 Published online by Cambridge University Press

also on conditions at the base including the basal-ice and subglacial rheology, hydrology and till availability. These basal conditions are poorly mapped beneath the Antarctic ice sheets but are collectively represented in IFPA by a mean non-dimensional slipperiness parameter, $\bar{C}$. Here, building from Ockenden and others (2022) and Kyrke-Smith and others (2017), we use $\bar{C}$ as a tuneable parameter to constrain the amplitude of the topography, and explore optimal values for basal slipperiness across different parts of the glacier. We therefore ran the model with respective mean-slipperiness values of $\bar{C} = 25$, 50, 75, 100, 150 and 200.

In order to evaluate the best value of mean non-dimensional slipperiness $\bar{C}$, we compare the bed topography across Pine Island Glacier from IFPA to (a) 3D ice-penetrating radar-sounded bed topography acquired in 2013/14 and (b) 2D airborne-radar-sounded bed topography acquired in 2004/05 (Vaughan and others, 2006; Jordan and Robinson, 2021). Because, mathematically, IFPA cannot resolve features aligned to the ice-flow direction ($k = 0$), we only examine results for radar lines oriented at an angle of less than 10 degrees to flow. These lines primarily sound across-flow features which should be resolved.

3. Results

3.1. Full-Stokes vs shallow-ice-stream approximation

Figure 1 shows a comparison of the bed topography from the IFPA model when run with the full-Stokes transfer functions and the shallow-ice-stream transfer functions, with all other parameters kept constant between the two model runs. We know from Gudmundsson (2008) that, compared to the full-Stokes equations, the shallow-ice-stream approximation underestimates bed topography for wavelengths less than about 10 ice thicknesses (roughly 20 km in this case) when inverting from the ice surface. We can see in Figure 1 that the full-Stokes transfer functions generally produce higher amplitude topography, in agreement with the theory. Gudmundsson (2008) also shows that this underestimation depends on the ice surface slope, and the basal slip ratio, which is most likely why the differences in amplitude are higher closer to the grounding line. Since meso-scale (2–30 km) bedforms are some of the features which we are most interested to estimate with this method, the rest of the results presented in this paper use the full-Stokes transfer functions from Gudmundsson (2003).

3.2. Modelled bed topography

Figure 2 shows the bed topography derived from IFPA, compared with bed topography directly surveyed with radar and modelled from flowline diffusion in Bedmachine Antarctica. The results show that IFPA is successful in resolving medium-wavelength features which are not resolved by the flowline diffusion method. This is illustrated by the 5 km-wide subglacial hill in the centre of Site iSTARt1 (Fig. 2a) which is not present at all in Bedmachine Antarctica, the subglacial hill at the southwestern corner of Site iSTARt6 (Fig. 2b), and the 10 km-wide valley running from south to north (right to left) in the centre of Site iSTARt9 (Fig. 2c).

For features in the bed to make an impression on the ice surface, they need to have a wavelength which is at least equivalent to the thickness of the ice, which in the Pine Island region is around 2 km. Step functions have both long and short wavelength components, which means that sharp transitions in bed topography occurring over less than 2 km, such as the 400 m high cliff at Site iSTARt7 (Fig. 2d), tend to become more smoothed in the bed topography produced by IFPA, although they are still present. Smaller-scale features (or spikes) with no long-wavelength component, such as the subglacial hillocks in the western (lower in page) part of Site iSTARit (Fig. 2e), are completely smoothed out. Ice flow in Site iSTARit (Fig. 2e) is very slow, which also reduces transmission of basal variability to the ice surface. Synthetic tests (Gudmundsson, 2003, 2008; Ockenden and others, 2022) show that these small-scale spikes and bumps are features which are not large enough to make an impression on the ice surface, and will only have a local influence on basal ice flow.

Synthetic experiments have shown that for features in the bed to make an impression on the ice surface, they should be aligned in a direction offset from the flow direction by at least 10 degrees (Ockenden and others, 2022). Landforms with wavenumber combinations which correspond to features aligned to flow ($k = 0$) are not resolved, as they fall into the null space of the inversion. We therefore do not expect flow-parallel features, such as the mega-scale glacial lineations observed at Site 2010tr (Fig. 2f), to be resolved in the bed topography produced by IFPA, although there is a wider flow-parallel feature through this site in the IFPA topography. Features with a combination of different orientations, such as the lineated north-south ridge at Site iSTARt5 (Fig. 2g), can be partly identified. The deeper groove on the south (right) side of the ridge is not resolved, as it is aligned with the ice flow ($k = 0$). However, the crest of the ridge (top right to bottom left) is picked out well, as it is at an angle of around 45° to the ice flow.

3.3. Basal slipperiness

Figure 3 shows bed-topography cross-sections from the 2010–2014 ice-penetrating radar sites, and the comparison with the modelled bed topography with different values of the mean slipperiness, $\bar{C}$. For each site, we visually judge the best-fit value of mean non-dimensional slipperiness, $\bar{C}$, to be the result with the most similar amplitude to the ice-penetrating-radar-sounded bed at the maximum point of the most distinct hill or trough in the cross-section, and label this on each cross-section.

For Site iSTARt1 (Fig. 3a) and Site 2010tr (Fig. 3f), there is a clear best fit across the main hill feature. For Site iSTARt6 (Fig. 3b) we use the hill which goes off the side of the patch as the calibration feature. In some lines (e.g. Figs 3c, 3d) we can not resolve all the small-scale variability and so we compare to the broader-scale topographic shapes. For Site iSTARt5 (Fig. 3g) the topography does not have any particularly distinct features, and so we use the mean non-dimensional slipperiness value of $\bar{C} = 100$. For Site iSTARit (Fig. 3e) none of the model runs can reproduce the amplitude of the hill in the centre of the transect. For the purposes of mapping variability, we suggest an extremely low slipperiness of $\bar{C} = 5$, but in reality the slow flow of ice in this patch probably means that the ice surface does not fully reflect the bed in this region and so IFPA can not resolve the bed topography.

Figure 4 shows the bed-topography cross-sections from selected airborne radar profiles, and comparison with the different values of the mean slipperiness $\bar{C}$. Some of these profiles (Figs 4c, 4e, 4g, 4i, 4j, 4k, 4i, 4m, 4n, 4q) closely fit the radar-sounded bed topography such that the selection of the mean non-dimensional slipperiness $\bar{C}$ is straightforward. For two profiles (Figs 4a, 4f), the positions of the amplitude maxima are not the same in the airborne radar and the inverted bed topography, but we pick the maximum amplitude of the inverted topography which lines up best. For the rest of the selected airborne-radar profiles (Figs 4b, 4d, 4h, 4o, 4p, 4r), the overall amplitude of the topography is correct but some of the shorter-scale features are not resolved.

Putting together the best-fit values for each cross-section leads to a map of mean non-dimensional slipperiness, $\bar{C}$ (Fig. 5) across

https://doi.org/10.1017/jog.2023.50 Published online by Cambridge University Press

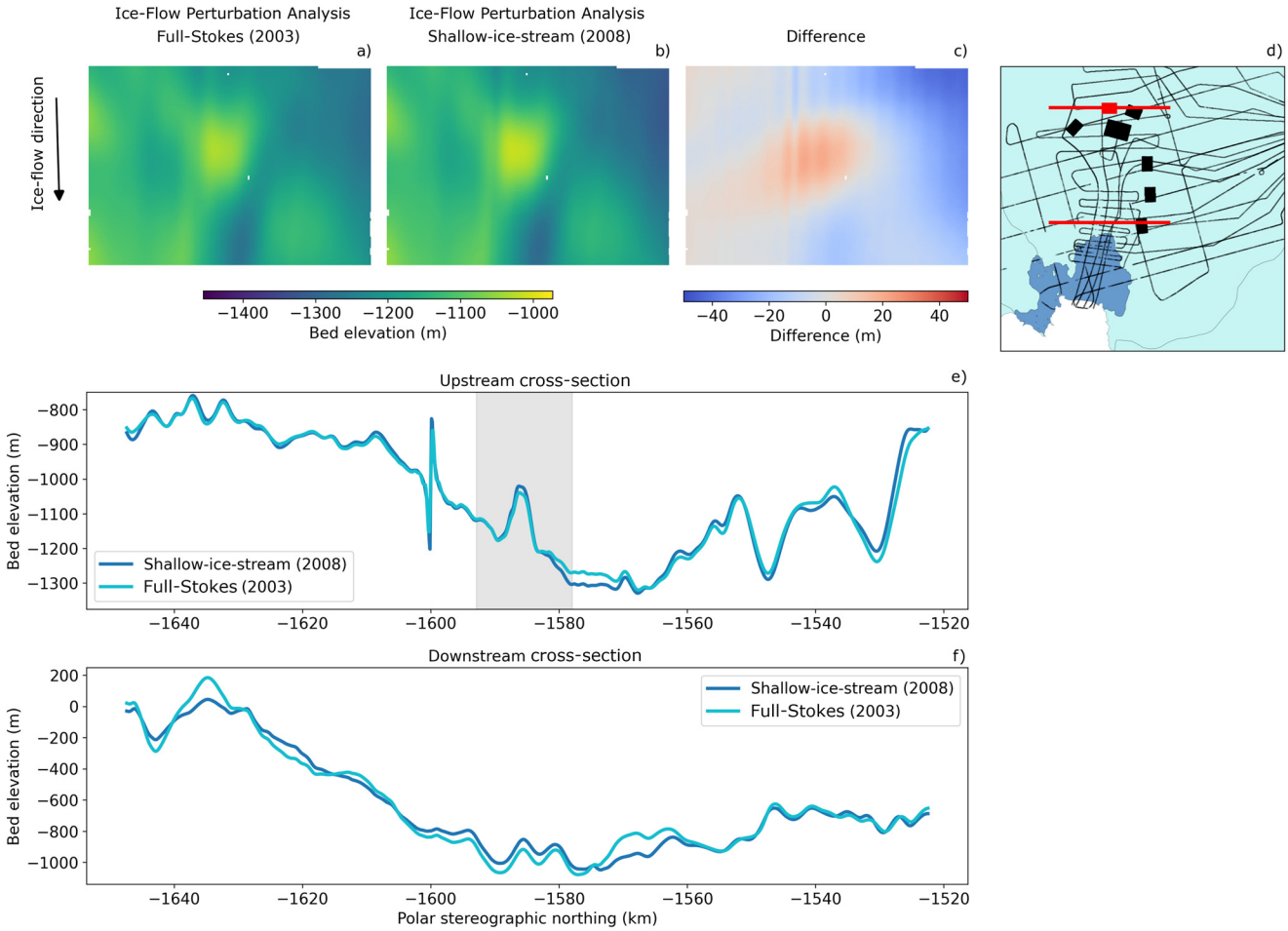

Figure 1. A comparison of bed topography produced from Ice-Flow Perturbation Analysis (IFPA) with the full-Stokes transfer functions from Gudmundsson (2003) and the shallow-ice-stream transfer functions from Gudmundsson (2008) for a 3D topographic patch (Site iSTARt1), and two linear cross-sections. Mean non-dimensional slipperiness, $\bar{C} = 100$. (d) Location figure marking patches of 3-D topography surveyed at high resolution with ice-penetrating radar in 2013/14 (Bingham and others (2017); black rectangles, with the patch in panels a–c coloured red), and airborne-radar profiles acquired in 2004/05 (Vaughan and others (2006); black lines, with red lines marking profiles in panels e and f). Panel (e) shows the comparison for the upstream cross-section, and panel (f) shows the comparison for the downstream cross-section. The grey highlighted section of panel (e) marks the profile's transition across Site iSTARt1. Spikes at −1600 km in panel (e) result from an artefact of the transition between tiles of the REMA data, which could be avoided by using a continuous surface elevation product.

the main trunk of Pine Island Glacier. The dimensional slipperiness, $\bar{c}$, is shown in Figure 5b, but this is mostly dominated by the velocity (which is a component in the dimensionalisation) and so does not necessarily show localised variability.

4. Discussion

4.1. Assessing IFPA performance through comparison to radar surveys

The overall performance of IFPA as applied to the radar-sounded topography on Pine Island Glacier for this paper is consistent with our understanding of IFPA from synthetic tests (Ockenden and others, 2022). Mathematically, we do not expect to be able to resolve features aligned to ice flow ($k = 0$) or smaller horizontal extent than the ice thickness, and indeed we do not. Features which do not fall into either of these two categories are, however, resolved well, and in a number of locations represent topography that is not resolved in the interpolated bed topography from Bedmachine Antarctica (e.g. Fig. 2a).

For all of the sites discussed in this paper, Bedmachine Antarctica uses a method termed 'flowline diffusion' to interpolate bed topography. Flowline diffusion is an anistropic interpolation method 'not based on physics' (Morlighem and others, 2020, SI pg6) which allows more variability across flow than along flow, thereby preserving features aligned with the ice-flow direction ($k = 0$). Interpolation occurs between radar lines, which are often spaced more than 5 km apart. There is no allowance for features which are not aligned to flow, and which do not cross one of these radar lines, and so we would not expect flowline diffusion, and hence Bedmachine Antarctica, to be able to detect features such as the subglacial hills in Site iSTARt1 and Site iSTARt6 (Figs 2a, 2b), or the valley in Site iSTARt9 (Fig. 2c). IFPA therefore offers the potential to improve our knowledge of bed topography in parts of Antarctica where features exist between radar survey lines and have an expression in the ice surface.

4.2. Exploring the role of the tuneable slipperiness parameter $\bar{C}$

In this work, we have also explored how we can use existing radar-sounded bed topography to explore the role of the mean slipperiness parameter, $\bar{C}$, and its effects on the amplitude of the topography. Typically, basal slipperiness is modelled by inverting surface observations with a fixed bed topography (Morlighem and others, 2010). Nias and others (2016) adopt an iterative approach starting with BedMap2 to produce topography and friction maps for the Amundsen Bay Embayment. Some models invert for slipperiness and topography together, but these have not been applied to Pine Island Glacier. If there are errors in

https://doi.org/10.1017/jog.2023.50 Published online by Cambridge University Press

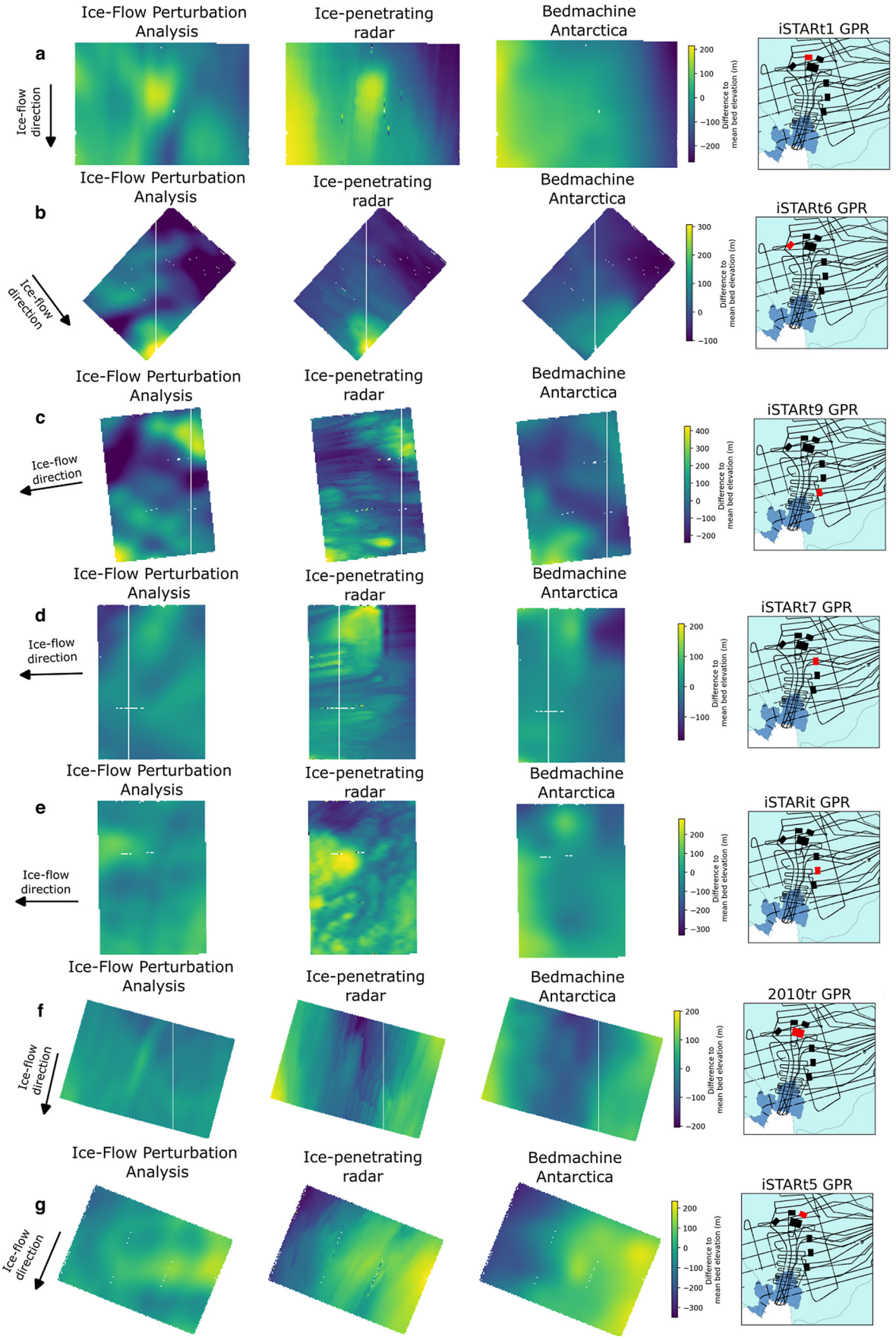

Figure 2. A comparison of bed topography from IFPA, ice-penetrating radar and BedMachine Antarctica flowline-diffusion interpolation for seven regions of Pine Island Glacier. (a) iSTARt1, (b) iSTARt6, (c) iSTARt9, (d) iSTARt7, (e) iSTARit, (f) 2010tr and (g) iSTARt5. IFPA plots are for the best fit value of $\bar{C}$, as shown in Figure 3. ($\bar{C}$ = 75, 50, 25, 150, 5, 200, 100 from top to bottom). Survey-site locations are shown in red in the rightmost column.

https://doi.org/10.1017/jog.2023.50 Published online by Cambridge University Press

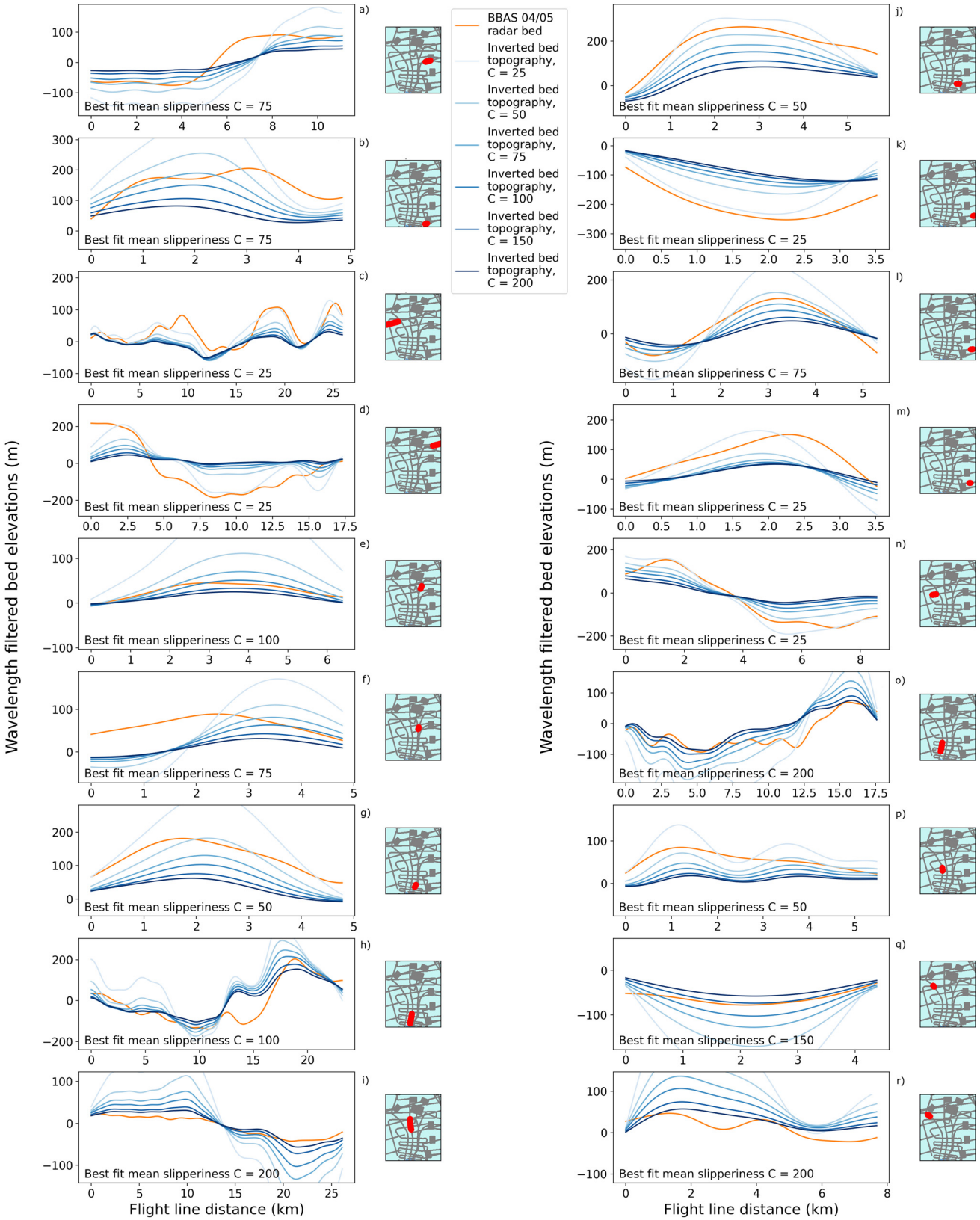

Figure 4. Bed topography profiles (with wavelengths >50 km removed) from selected airborne-radar profiles which are at angles of no more than 10 degrees to flow and contain distinct bedforms (panels a– r). The radar bed pick is shown in orange and the IFPA beds for different values of the mean slipperiness parameter $\bar{C}$ are in graduated shades of blue. Profile locations are shown in red on the inset maps.

the bed topography, these then propagate into the slipperiness estimate. Kyrke-Smith and others (2017) showed that including high-resolution topography can reduce the modelled basal slipperiness, as it changes the way basal drag is partitioned in these inversions. The total basal friction is partitioned between form drag (caused by topography) and skin drag (caused by other basal properties), so more knowledge about topography can increase the modelled contribution from form drag, but decrease

https://doi.org/10.1017/jog.2023.50 Published online by Cambridge University Press

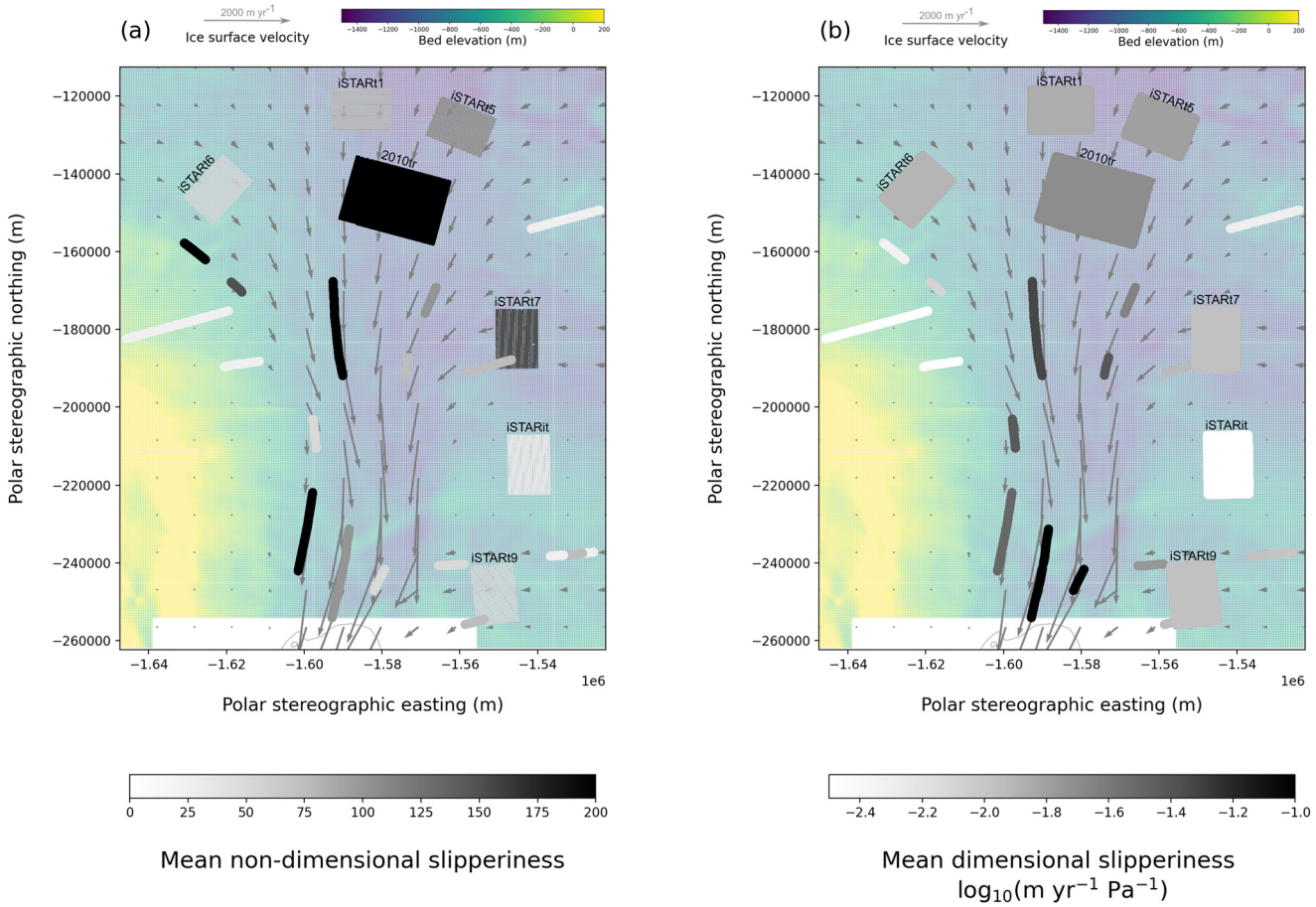

Figure 5. The best-fit mean slipperiness across Pine Island Glacier, as calculated by comparing the amplitude of landforms observed in radar measurements to those from IFPA, with bed topography and ice-surface velocity shown in the background. Both the airborne radar lines and ice-penetrating radar grids are shown. (a) Non-dimensional slipperiness, (b) dimensional slipperiness (note that this mostly varies with velocity). Higher slipperiness is observed in the main trunk and tributaries. Due to the mathematical inability of IFPA to resolve landforms aligned to flow ($k = 0$), only radar lines aligned to flow (which cross landforms at an angle to flow) have been used.

the modelled skin drag contribution, which is what the basal slipperiness parameter represents. Modelled slipperinesses which use the bed topography from BedMap2 (Morlighem and others, 2010; De Rydt and others, 2013; Kyrke-Smith and others, 2017) or Bedmachine Antarctica (Barnes and others, 2021) are likely to overestimate the contribution from skin drag, and may falsely attribute this to bed properties such as water content or till distributions. The method which we apply here to map the basal slipperiness only uses direct observations of topography rather than interpolated topography, and therefore avoids this issue. It does require accurate bed measurements to be available in the local area for calibration, but topographic measurements from other tributaries to the same glacier, or nearby glaciers should be sufficient, as long as the geology is thought to be similar.

Figure 5 depicts a general trend for higher slipperiness in the main trunk of the glacier, and lower slipperiness in the higher topographic regions between the tributaries. A higher slipperiness means lower friction for sliding, and we propose that this is likely to be due to higher erosion rates and a thicker sediment layer in the main glacial trough, such as at Site 2010tr (Fig. 3f) and some of the airborne survey lines (e.g. Figs 4h, 4n). Lower slipperiness means more friction against sliding, and we suggest this is likely to be due to more exposed bedrock on the higher topography, for example at Site iSTARt9 (Fig. 3c), and the airborne-radar profiles shown in Figures 4b and 4c. As well as agreeing with other modelled basal-slipperiness studies (Morlighem and others, 2010; De Rydt and others, 2013; Kyrke-Smith and others, 2017; Barnes and others, 2021), this is what we would expect in an active glacial environment, where the motion of the ice erodes glacial till. The till is removed from the higher topography exposing the bedrock, and accumulates in glacial troughs, where it can lubricate ice flow. Seismic studies from Pine Island Glacier (Smith and others, 2013; Brisbourne and others, 2017; Davies and others, 2018) and offshore work in Pine Island Bay (Nitsche and others, 2013; Muto and others, 2016) also support this picture of a mixed subglacial environment with abundant till and some exposed bedrock.

4.3. Applying Ice-Flow Perturbation Analysis to other regions of Antarctica

We have found that there is considerable variation in the values of IFPA-inferred mean slipperiness which match best with the existing bed topography across Pine Island, but this variability appears to be linked with broad-scale topographic patterns. Bingham and others (2017) showed that there was a first-order relationship between bed topography and ice flow across Pine Island Glacier, pointing to the principal importance of form drag. Seismic surveys (Smith and others, 2013; Brisbourne and others, 2017) support these findings and have suggested that there is a connection between topography, the distribution of glacial tills and sliding patterns. A relationship between bed-sliding properties and topography has also been observed on Thwaites Glacier (Muto and others, 2019a, 2019b; Clyne and others, 2020). Due to the spread of best-fit mean slipperiness values, we propose that a spatially variable mean slipperiness parameter, $\bar{C}$, should be used when

https://doi.org/10.1017/jog.2023.50 Published online by Cambridge University Press

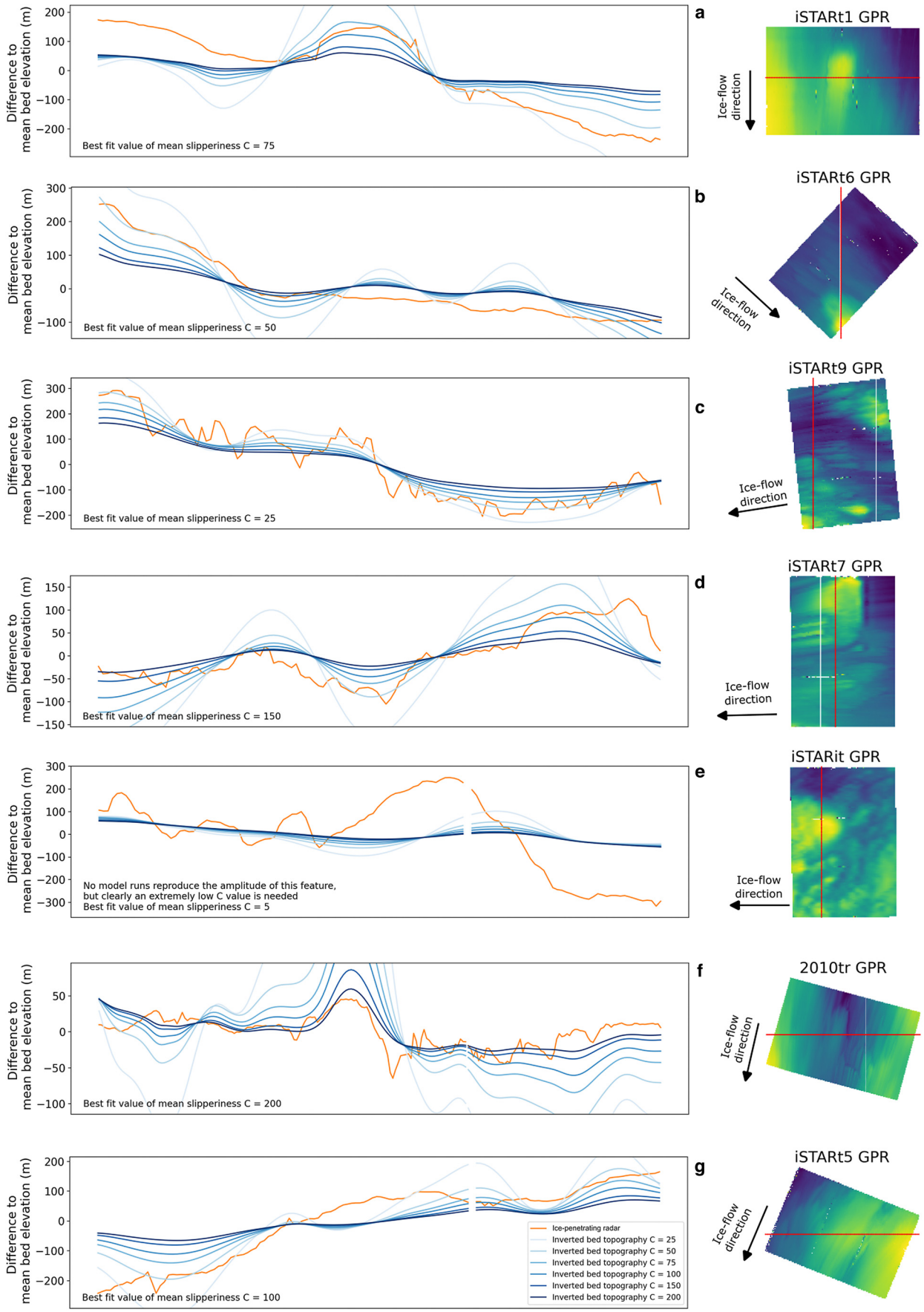

Figure 3. Cross-sections across the main topographic features in each of the radar-survey sites: (a) iSTARt1, (b) iSTARt6, (c) iSTARt9, (d) iSTARt7, (e) iSTARit, (f) 2010tr and (g) iSTARt5. The amplitudes of the IFPA results are shown for different values of the mean slipperiness parameter $\bar{C}$ in graduated shades of blue, and the ice-penetrating radar results in orange. Cross-section profile locations are marked red over the radar-sounded topographic maps. White lines are data gaps which arise due to interpolation. Comparison between the radar surveys and different model runs allows for an assessment of the best-fit mean slipperiness at each site (shown in the bottom-left), and therefore slipperiness variability across the Pine Island Glacier region.

https://doi.org/10.1017/jog.2023.50 Published online by Cambridge University Press

applying IFPA to other regions of Antarctica. Ideally, a local constraint on the variations in $\bar{C}$ should be used, but since there are relatively few areas with such high-density radar surveys to use for this calibration in other regions, we propose applying values of $\bar{C} = 150$ in glacial troughs and $\bar{C} = 50$ in rougher areas in between. This may lead to a slight overestimate of topography in troughs and an underestimate between them, but should account for some of the difference in sliding mechanics, and produce more realistic bed topography overall.

When considering the regions of Antarctica where IFPA might be useful, it is important to consider the known weaknesses of the method. In regions of extremely slow flowing ice, such as Site iSTARit (Fig. 3e), even extremely low values of the mean non-dimensional slipperiness can not match the existing bed topography. The IFPA method assumes that the ice surface is in steady state with the bed, but we suggest that this mismatch may be due to the slow transfer of the topographic variability from the bed to the surface. Although these slow flowing regions are not terribly important in contemporary ice dynamics, they may become important in the future as regions of faster flow expand further inland from the current coastline. More intriguingly, however, they may also give a hint of how palaeo-ice-dynamics could have been different. Analysis of the relationship between englacial stratigraphy and both the 'true' radar topography and the modelled IFPA topography in these regions has the potential to further illuminate past variations in ice-flow patterns.

Another issue with IFPA is that we require a continuous 50 km by 50 km patch which can be approximated by flow in an inclined slab, in order to invert the surface elevation and velocity fields. This means that we can not apply the method too close to the grounding line, as floating ice behaves with different physics to grounded ice. However, in fast flowing ice close to the grounding line where dense radar observations are available, Bedmachine Antarctica uses the mass conservation method, which takes into account variation in surface elevation (Morlighem and others, 2020) and is therefore less likely to miss mesoscale landforms than the flowline diffusion method which is used further inland. Requiring flow which can be approximated by slab flow also means that IFPA is likely to struggle in regions where the ice is not fully covering the topography at the 50 km scale, such as in the Antarctic Peninsula. It is possible to reduce the size of the patch, which may increase the utility of the method in smaller glaciers, as long as the ice thickness is much less than the width between confining walls so that the flow can be approximated by an inclined slab. Generally though, we believe that the IFPA method will be of most use in inland regions with continuous ice cover.

IFPA tells us about variations in the bed relative to the mean elevation, but does not tell us about the absolute ice thickness. To demonstrate the potential of the method, and to ensure that we present an independent test of IFPA and Bedmachine Antarctica, we have used a single ice-thickness value for each 50 km by 50 km region in the Pine Island Glacier catchment. However, to improve the utility of the IFPA bed-topography product, we could incorporate more of the measured radar bed topography which is included in Bedmachine Antarctica, potentially using the error estimate which accompanies Bedmachine Antarctica. The strength of flowline diffusion is the ability to interpolate along flow landforms, which is one of the known weaknesses of IFPA. A combined product which includes both the flow-oriented landforms from Bedmachine Antarctica and the flow-orthogonal landforms from IFPA would represent a powerful baseline for the next generation of ice-sheet models, for which the representation of basal roughness and traction is so crucial (e.g. Durand and others, 2011; Kyrke-Smith and others, 2018; Nias and others, 2018).

5. Conclusions

Building on the work of Gudmundsson (2003); Gudmundsson and Raymond (2008) and Thorsteinsson and others (2003), and our recent application of IFPA on Thwaites Glacier (Ockenden and others, 2022), we have produced maps of the bed topography beneath Pine Island Glacier, West Antarctica, by inverting from satellite-derived surface ice properties and varying values of basal slipperiness. We use transfer functions for IFPA based on the full-Stokes equations rather than the shallow-ice-stream approximation. A comparison of the inverted topography with directly sounded topography from ice-penetrating radar and the bed interpolated using flowline diffusion in Bedmachine Antarctica shows that our application of IFPA is able to capture topographic features which could never be resolved by flowline diffusion. Since flowline diffusion is the main method used by Bedmachine Antarctica in the inland regions of Antarctica, IFPA offers the potential to enhance our understanding of bed topography across much of the continent.

We also used the trade-off between mean slipperiness $\bar{C}$, and topographic amplitude in the IFPA method to explore trends in slipperiness across the main trunk and tributaries of Pine Island Glacier. We found higher slipperiness (or lower basal friction) in the main glacial trough and lower slipperiness (or higher basal friction) on the elevated topography between tributaries; this trend agrees with observations from seismic surveys. Matching the radar topography with IFPA requires a range of values of the mean slipperiness parameter. When applying IFPA in other regions of Antarctica, we would ideally use local radar observations for calibrating $\bar{C}$, but in areas with sparsely distributed radar measurements, we suggest applying a variable mean slipperiness of $\bar{C} = 150$ in fast-flowing glacial troughs and $\bar{C} = 50$ in slower-moving highlands.

Supplementary material. The supplementary material for this article can be found at https://doi.org/10.1017/jog.2023.50

Data. The code used for IFPA over Pine Island Glacier is available on github and zenodo at (https://doi.org/10.5281/zenodo.8085778). The data for plotting the figures in this article are available on zenodo at (https://doi.org/10.5281/zenodo.8085878). The surface elevation data from REMA (Howat and others, 2019), velocity data from ITS_LIVE (Gardner and others, 2018) and BedMachine Antarctica bed topography (Morlighem and others, 2020) datasets used are available online.

Acknowledgements. This work is an output of the NERC E4 Doctoral Training Partnership at the University of Edinburgh and the Geophysical Habitat of Subglacial Thwaites (GHOST) project, a component of the International Thwaites Glacier Collaboration (ITGC). This research has been supported by the Natural Environment Research Council (grant nos. NERC NE/S007407, NERC NE/S006672, NERC NE/S006621/1, NERC NE/S006613/1, NERC NE/S006796/1) and the National Science Foundation (grant no. NSF PLR 1738934).

References

Balise MJ and Raymond CF (1985) Transfer of basal sliding variations to the surface of a linearly viscous glacier. *Journal of Glaciology* **31**(109), 308–318. doi: 10.3189/s002214300000664x

Barnes JM and 5 others (2021) The transferability of adjoint inversion products between different ice flow models. *The Cryosphere* **15**(4), 1975–2000. doi: 10.5194/tc-15-1975-2021

Bingham RG and 12 others (2017) Diverse landscapes beneath Pine Island Glacier influence ice flow. *Nature Communications* **8**(2017), 1618. doi: 10.1038/s41467-017-01597-y

Brisbourne AM and 8 others (2017) Bed conditions of Pine Island Glacier, West Antarctica. *Journal of Geophysical Research: Earth Surface* **122**(1), 419–433. doi: 10.1002/2016JF004033

Budd W (1970) Ice flow over bedrock perturbations. *Journal of Glaciology* **9**(55), 29–48. doi: 10.3189/s0022143000026770

Clyne ER, Anandakrishnan S, Muto A, Alley RB and Voigt DE (2020) Interpretation of topography and bed properties beneath Thwaites Glacier, West Antarctica using seismic reflection methods. *Earth and Planetary Science Letters* **550**, 116543. doi: 10.1016/j.epsl.2020.116543

Cooper MA, Jordan TM, Siegert MJ and Bamber JL (2019) Surface expression of basal and englacial features, properties, and processes of the Greenland Ice Sheet. *Geophysical Research Letters* **46**(2), 783–793. doi: 10.1029/2018GL080620

Davies D and 8 others (2018) How dynamic are ice-stream beds?. *The Cryosphere* **12**(5), 1615–1628. doi: 10.5194/tc-12-1615-2018

De Rydt J, Gudmundsson G, Corr H and Christoffersen P (2013) Surface undulations of Antarctic ice streams tightly controlled by bedrock topography. *The Cryosphere* **7**(2), 407–417. doi: 10.5194/tc-7-407-2013

Durand G, Gagliardini O, Favier L, Zwinger T, le Meur E (2011) Impact of bedrock description on modeling ice sheet dynamics. *Geophysical Research Letters* **38**(20), L20501. doi: 10.1029/2011GL048892

Fretwell P and 59 others (2013) Bedmap2: improved ice bed, surface and thickness datasets for Antarctica. *The Cryosphere* **7**(1), 375–393. doi: 10.5194/tc-7-375-2013

Gardner AS and 6 others (2018) Increased West Antarctic and unchanged East Antarctic ice discharge over the last 7 years. *The Cryosphere* **12**(2), 521–547. doi: 10.5194/tc-12-521-2018

Gudmundsson GH (2003) Transmission of basal variability to a glacier surface. *Journal of Geophysical Research: Solid Earth* **108**(B5), 2253. doi: 10.1029/2002JB002107

Gudmundsson GH (2008) Analytical solutions for the surface response to small amplitude perturbations in boundary data in the shallow-ice-stream approximation. *The Cryosphere* **2**(2), 77–93. doi: 10.5194/tc-2-77-2008

Gudmundsson GH and Raymond M (2008) On the limit to resolution and information on basal properties obtainable from surface data on ice streams. *The Cryosphere* **2**(2), 167–178. doi: 10.5194/tc-2-167-2008

Howat IM, Porter C, Smith BE, Noh MJ and Morin P (2019) The reference elevation model of Antarctica. *The Cryosphere* **13**(2), 665–674. doi: 10.5194/tc-13-665-2019

Ignéczi Á, Sole AJ, Livingstone SJ, Ng FSL and Yang K (2018) Greenland ice sheet surface topography and drainage structure controlled by the transfer of basal variability. *Frontiers in Earth Science* **6**, 101. doi: 10.3389/feart.2018.00101

Jordan T and Robinson C (2021) Bed, surface elevation and ice thickness measurements derived from radar data acquired during the Thwaites Glacier airborne survey (2019/2020) (Version 1.0) [Data set]. *NERC EDS UK Polar Data Centre* (doi: 10.5285/7c12898d-7e55-458c-ba7d-ecec8252f3b5).

Kyrke-Smith TM, Gudmundsson GH and Farrell PE (2017) Can seismic observations of bed conditions on ice streams help constrain parameters in ice flow models?. *Journal of Geophysical Research: Earth Surface* **122**(11), 2269–2282. doi: 10.1002/2017JF004373

Kyrke-Smith T, Gudmundsson G and Farrell P (2018) Relevance of detail in basal topography for basal slipperiness inversions: a case study on Pine Island Glacier, Antarctica. *Frontiers in Earth Science* **6**, 33. doi: 10.3389/feart.2018.00033

Morlighem M and 5 others (2010) Spatial patterns of basal drag inferred using control methods from a full-Stokes and simpler models for Pine Island Glacier, West Antarctica. *Geophysical Research Letters* **37**(14), L14502. doi: 10.1029/2010GL043853

Morlighem M and 36 others (2020) Deep glacial troughs and stabilizing ridges unveiled beneath the margins of the Antarctic ice sheet. *Nature Geoscience* **13**(2), 132–137. doi: 10.1038/s41561-019-0510-8

Muto A and 6 others (2016) Subglacial bathymetry and sediment distribution beneath Pine Island Glacier ice shelf modeled using aerogravity and in situ geophysical data: new results. *Earth and Planetary Science Letters* **433** (2016), 63–75. doi: 10.1016/j.epsl.2015.10.037

Muto A and 7 others (2019b) Relating bed character and subglacial morphology using seismic data from Thwaites Glacier, West Antarctica. *Earth and Planetary Science Letters* **507**(2019), 199–206. doi: 10.1016/j.epsl.2018.12.008

Muto A, Alley RB, Parizek BR and Anandakrishnan S (2019a) Bed-type variability and till (dis)continuity beneath Thwaites Glacier, West Antarctica. *Annals of Glaciology* **60**(80), 82–90. doi: 10.1017/aog.2019.32

Ng FSL, Ignéczi D, Sole AJ and Livingstone SJ (2018) Response of surface topography to basal variability along glacial flowlines. *Journal of Geophysical Research: Earth Surface* **123**(10), 2319–2340. doi: 10.1029/2017JF004555

Nias IJ, Cornford SL and Payne AJ (2016) Contrasting the modelled sensitivity of the Amundsen Sea Embayment ice streams. *Journal of Glaciology* **62** (233), 552–562. doi: 10.1017/jog.2016.40

Nias IJ, Cornford SL and Payne AJ (2018) New mass-conserving bedrock topography for Pine Island Glacier impacts simulated decadal rates of mass loss. *Geophysical Research Letters* **45**(7), 3173–3181. doi: 10.1002/2017GL076493

Nitsche FO and 8 others (2013) Paleo ice flow and subglacial meltwater dynamics in Pine Island Bay, West Antarctica. *The Cryosphere* **7**(1), 249–262. doi: 10.5194/tc-7-249-2013

Nye JF (1959) The motion of ice sheets and glaciers. *Journal of Glaciology* **3** (26), 493–507. doi: 10.3189/s002214300001724x

Ockenden H, Bingham RG, Curtis A and Goldberg D (2022) Inverting ice surface elevation and velocity for bed topography and slipperiness beneath Thwaites Glacier. *The Cryosphere* **16**(9), 3867–3887. doi: 10.5194/tc-16-3867-2022

Reeh N (1987) Steady-state three-dimensional ice flow over an undulating base: first-order theory with linear ice rheology. *Journal of Glaciology* **33** (114), 177–185. doi: 10.3189/s0022143000008674

Smith AM, Jordan TA, Ferraccioli F and Bingham RG (2013) Influence of subglacial conditions on icestream dynamics: seismic and potential field data from Pine Island Glacier, West Antarctica. *Journal of Geophysical Research: Solid Earth* **118**(4), 1471–1482. doi: 10.1029/2012JB009582

Thorsteinsson T and 5 others (2003) Bed topography and lubrication inferred from surface measurements on fast-flowing ice streams. *Journal of Glaciology* **49**(167), 481–490. doi: 10.3189/172756503781830502

Vaughan DG and 9 others (2006) New boundary conditions for the West Antarctic ice sheet: subglacial topography beneath Pine Island Glacier. *Geophysical Research Letters* **33**(9), L09501. doi: 10.1029/2005GL025588

Whillans IM and Johnsen SJ (1983) Longitudinal variations in glacial flow: theory and test using data from the Byrd Station Strain Network, Antarctica. *Journal of Glaciology* **29**(101), 78–97. doi: 10.3189/s0022143000005165

https://doi.org/10.1017/jog.2023.50 Published online by Cambridge University Press

Supplement of Ice-Flow Perturbation Analysis: A method to estimate ice-sheet bed topography and conditions from surface datasets

Helen OCKENDEN,[1] Robert G BINGHAM,[1] Andrew CURTIS,[1] Daniel GOLDBERG[1]

[1] *School of GeoSciences, University of Edinburgh, Drummond St, Edinburgh, EH8 9XP*
Correspondence: Helen Ockenden <h.ockenden@sms.ed.ac.uk>

NON-DIMENSIONALISED TRANSFER FUNCTIONS

For ice in a planar slab aligned in the direction of ice flow, the non-dimensionalised Fourier transforms of perturbations in ice surface elevation, ($\hat{S}$), and velocity, ($\hat{U}$, $\hat{V}$), can be calculated from the non-dimensionalised Fourier transforms of perturbations in bed topography, ($\hat{B}$), and basal slipperiness, ($\hat{C}$):

$$\hat{S}(k,l) = T_{SB}(k,l)\,\hat{B}(k,l) + T_{SC}(k,l)\,\hat{C}(k,l), \tag{1}$$

$$\hat{U}(k,l) = T_{UB}(k,l)\,\hat{B}(k,l) + T_{UC}(k,l)\,\hat{C}(k,l), \tag{2}$$

$$\hat{V}(k,l) = T_{VB}(k,l)\,\hat{B}(k,l) + T_{VC}(k,l)\,\hat{C}(k,l), \tag{3}$$

where T_{sb}, T_{sc}, T_{ub}, T_{uc}, T_{vb}, T_{vc} are wavenumber specific non-dimensional transfer functions which describe the amplitude ratio of perturbations in the bed properties relative to the ice surface properties, and which vary with the wavenumbers k and l, angle of slope, α, sliding law parameter, m, and mean non-dimensionalised bed slipperiness, $\bar{C}$.

Depending on whether full-Stokes flow (Gudmundsson, 2003) or the shallow-ice-stream approximation (Gudmundsson, 2008) are considered, these transfer functions take different functional forms, where $j^2 = k^2 + l^2$.

For the shallow-ice-stream approximation (Gudmundsson, 2008)

$$T_{SB}(k,l) = \frac{k\left(1 + m\left(2j^2\bar{C} + 1\right)\right)}{k + m\left(k + 2kj^2\bar{C} + \mathrm{i}j^2\cot\alpha\right)}, \tag{4}$$

$$T_{UB}(k,l) = \frac{-\mathrm{i}\cot\alpha\left(l^2 m - k^2\left(1 + 0.5j^2 m\bar{C}\right)\right)}{\left(k + m\left(k + 2kj^2\bar{C} + \mathrm{i}j^2\cot\alpha\right)\right)\left((m\bar{C})^{-1} + 0.5j^2\right)}, \tag{5}$$

$$T_{VB}(k,l) = \frac{\mathrm{i}kl\left(1 + 0.5j^2 mC + m\right)\cot\alpha}{\left(k + m\left(k + 2kj^2\bar{C} + \mathrm{i}j^2\cot\alpha\right)\right)\left((m\bar{C})^{-1} + 0.5j^2\right)}, \tag{6}$$

$$T_{SC}(k,l) = \frac{k}{k + m\left(k + 2kj^2\bar{C} + \mathrm{i}j^2\cot\alpha\right)}, \tag{7}$$

$$T_{UC}(k,l) = \frac{\bar{C}\left(3kl^2 m\bar{C} + 2k + kj^2 m\bar{C} + 2il^2\cot\alpha m\right)}{\left(k + m\left(k + 2kj^2\bar{C} + \mathrm{i}j^2\cot\alpha\right)\right)\left(2 + j^2 m\bar{C}\right)}, \tag{8}$$

$$T_{VC}(k,l) = \frac{-klm\bar{C}\left(2i\cot\alpha + 3k\bar{C}\right)}{\left(k + m\left(k + 2kj^2\bar{C} + \mathrm{i}j^2\cot\alpha\right)\right)\left(2 + j^2 m\bar{C}\right)}. \tag{9}$$

For full-Stokes flow (Gudmundsson, 2003)

$$T_{SB}(k,l) = \frac{jk\Big((1+\bar{C})\big(\bar{C}j\sinh(j)+\cosh(j)\big)+\cosh(j)\big(1+\bar{C}+\bar{C}^2j^2\big)\Big)}{jk(1+\bar{C})\Big(\cosh(j)\big(\bar{C}j\sinh(j)+\cosh(j)\big)+1+j^2\big(1+\bar{C}\big)\Big) + i\cot(\alpha)\Big(\big(Cj\sinh(j)+\cosh(j)\big)\sinh(j)-j\Big)}, \tag{10}$$

$$\begin{aligned} T_{UB,num}(k,l) = &\Big(\sinh^2(j)\Big(j^2\cot(\alpha)\sinh(j)\cosh(j)\Big(\bar{C}\big(2-k^2(\bar{C}^2j^2+4+\bar{C})\big)+4\Big) \\ &+ ik\Big(j^4\bar{C}\Big(3\bar{C}k^2(1+\bar{C})-4\Big)+2\Big(j^2\big(k^2(4\bar{C}+2+\bar{C}^2)+4+4\bar{C}\big)-2k^2(1+\bar{C})\Big) \\ &+ j^3\Big(\bar{C}^3j^2\big(k^2(1+\bar{C})+2\big)+\bar{C}k^2\big(5\bar{C}+4\big)+2\big(3\bar{C}-2\big)\big(1+\bar{C}\big)\Big)-4k^2j\bar{C}(1+\bar{C})\Big) \\ &+ j\cot(\alpha)\Big(\big(-3\bar{C}^2k^2+2\bar{C}(2+\bar{C})\big)j^2-k^2(2+\bar{C})^2\Big)\Big)-2j^3\cot(\alpha)\Big(\bar{C}^2k^2+\bar{C}+2\Big) \\ &+ 2ikj\Big(j^2\Big(k^2\big(5\bar{C}^2+6\bar{C}+2\big)-4-4\bar{C}\Big)-j^4\Big(2+5\bar{C}+4\bar{C}^2\Big)+2k^2\Big(1+\bar{C}\Big)\Big)\Big), \end{aligned} \tag{11}$$

$$\begin{aligned} T_{vel,den}(k,l) = &j^2\Big(j\cosh^3(j)\Big(ik(1+\bar{C})\Big(\bar{C}^2j^2+2\Big)-3\bar{C}\cot(\alpha)\Big) \\ &+ j\cosh(j)\Big(\cot(\alpha)\Big(2+3\bar{C}\Big)-ik(1+\bar{C})\Big(j^2\big(\bar{C}^2-2\bar{C}-2\big)-2\Big)\Big) \\ &+ \sinh^3(j)\Big(3ikj^2\bar{C}\Big(1+\bar{C}\Big)-\cot(\alpha)\Big(2+\bar{C}^2j^2\Big)\Big) \\ &+ \sinh(j)\Big(\cot(\alpha)\Big(j^2\bar{C}-2\Big)+ikj^2\bar{C}(1+\bar{C})\Big(j^2(1+\bar{C})+4\Big)\Big)\Big), \end{aligned} \tag{12}$$

$$T_{UB}(k,l) = T_{UB,num}(k,l) \,/\, T_{vel,den}(k,l), \tag{13}$$

$$\begin{aligned} T_{VB,num}(k,l) = &kl\Big(\sinh(j)\cosh(j)\Big(ik\Big(3\bar{C}^2j^4(1+\bar{C})+2j^2\big(2+4\bar{C}+\bar{C}^2\big)-4-4\bar{C}\Big) \\ &- j^2\bar{C}\cot(\alpha)\Big(j^2\bar{C}^2+\bar{C}+4\Big)\Big) \\ &+ \sinh^2(j)\Big(ikj\Big(\bar{C}^3j^4(1+\bar{C})+\bar{C}j^2\big(5\bar{C}+4\big)-4\bar{C}\big(1+\bar{C}\big)\Big) \\ &- j\cot(\alpha)\Big(3j^2\bar{C}^2+\big(2+\bar{C}\big)^2\Big)\Big) \\ &- 2\bar{C}^2j^3\cot(\alpha)+2ikj\Big(j^2\Big(5\bar{C}^2+6\bar{C}+2\Big)+2+2\bar{C}\Big)\Big), \end{aligned} \tag{14}$$

$$T_{VB}(k,l) = T_{VB,num}(k,l) \,/\, T_{vel,den}(k,l), \tag{15}$$

$$T_{SC}(k,l) = \frac{-\bar{C}kj\cosh(j)}{jk(1+\bar{C})\Big(\cosh(j)\big(\bar{C}j\sinh(j)+\cosh(j)\big)+1+j^2\big(1+\bar{C}\big)\Big) + i\cot(\alpha)\Big(\big(Cj\sinh(j)+\cosh(j)\big)\sinh(j)-j\Big)}, \tag{16}$$

(17)

$$
\begin{aligned}
T_{UC,num}(k,l) =& \bar{C}\Big(\sinh(j)\cosh(j)\Big(j^2\cot(\alpha)\Big(\bar{C}k^2-2\Big) \\
&+ ik\Big(2\bar{C}j^4(1+\bar{C}) - j^2\Big(k^2(2+\bar{C})(1+\bar{C})+4\Big)+2k^2\Big)\Big) \\
&+ j\sinh^2(j)\Big(\cot(\alpha)\Big(k^2(2+\bar{C})-2j^2\bar{C}\Big)+ik\Big(j^2\big(2-\bar{C}k^2(1+\bar{C})\big)+\bar{C}k^2\Big)\Big) \\
&+ 2j\Big(j^2\cot(\alpha)+ik\Big(j^4(1+\bar{C})^2+j^2\big(2+\bar{C}-k^2(1+\bar{C})^2\big)-k^2\Big)\Big)\Big), \qquad (18)
\end{aligned}
$$

$$
T_{UC}(k,l) = T_{UC,num}(k,l) \,/\, T_{vel,den}(k,l), \qquad (19)
$$

$$
\begin{aligned}
T_{VC,num}(k,l) =& -kl\bar{C}\Big(\sinh(j)\cosh(j)\Big(ik\Big(j^2\big(2+\bar{C}\big)\big(1+\bar{C}\big)-2\Big)-j^2\bar{C}\cot(\alpha)\Big) \\
&+ \sinh^2(j)\Big(ikj\bar{C}\Big(j^2(1+\bar{C})-1\Big)-\cot(\alpha)\Big(2+\bar{C}\Big)\Big)+2ijk\Big(j^2(1+\bar{C})^2+1\Big)\Big), \qquad (20)
\end{aligned}
$$

$$
T_{VC}(k,l) = T_{VC,num}(k,l) \,/\, T_{vel,den}(k,l). \qquad (21)
$$

REFERENCES

Gudmundsson GH (2003) Transmission of basal variability to a glacier surface. *Journal of Geophysical Research: Solid Earth*, **108**(B5), 2253 (doi: 10.1029/2002JB002107)

Gudmundsson GH (2008) Analytical solutions for the surface response to small amplitude perturbations in boundary data in the shallow-ice-stream approximation. *The Cryosphere*, **2**(2), 77–93, ISSN 1994-0424 (doi: 10.5194/tc-2-77-2008)